Effects of Hydrophobic Helix Length and Side Chain Chemistry on Biomimicry in Peptoid Analogues of SP-C†

Nathan J. Brown,‡ Cindy W. Wu,‡ Shannon L. Seurynck-Servoss,‡ and Annelise E. Barron*,§

Department of Chemical and Biological Engineering, Northwestern University, 2145 Sheridan Road, Evanston, Illinois 60208, and Department of Bioengineering, Stanford University, 318 Campus Drive, Stanford, California 94305

Received November 2, 2007; Revised Manuscript Received December 4, 2007

ABSTRACT: The hydrophobic proteins of lung surfactant (LS), SP-B and SP-C, are critical constituents of an effective surfactant replacement therapy for the treatment of respiratory distress syndrome. Because of concerns and difficulties associated with animal-derived surfactants, recent investigations have focused on the creation of synthetic analogues of the LS proteins. However, creating an accurate mimic of SP-C that retains its biophysical surface activity is extraordinarily challenging given the lipopeptide's extreme hydrophobicity and propensity to misfold and aggregate. One successful approach that overcomes these difficulties is the use of poly-N-substituted glycines, or peptoids, to mimic SP-C. To develop a non-natural, bioactive mimic of SP-C and to investigate the effects of side chain chemistry and length of the helical hydrophobic region, we synthesized, purified, and performed in vitro testing of two classes of peptoid SP-C mimics: those having a rigid α-chiral aromatic helix and those having a biomimetic α-chiral aliphatic helix. The length of the two classes of mimics was also systematically altered. Circular dichroism spectroscopy gave evidence that all of the peptoid-based mimics studied here emulated SP-C's secondary structure, forming stable helical structures in solution. Langmuir−Wilhelmy surface balance, fluorescence microscopy, and pulsating bubble surfactometry experiments provide evidence that the aromatic-based SP-C peptoid mimics, in conjunction with a synthetic lipid mixture, have superior surface activity and biomimetic film morphology in comparison to the aliphatic-based mimics and that there is an increase in surface activity corresponding to increasing helical length.

Lung surfactant (LS)[1] is a complex mixture of lipids and proteins found at the air−liquid interface within the lungs that is required for proper respiration. This unique biomaterial functions to reduce and regulate surface tension within the alveoli during respiration, greatly diminishing the work of breathing and preventing alveolar collapse. No single constituent of LS is solely responsible for its unique dynamic surface behavior. LS is composed of approximately 85−90% saturated and unsaturated phospholipids, 6−8% proteins, and 4−7% neutral lipids (*1*). Saturated phospholipids such as dipalmitoyl phosphatidylcholine (DPPC), the main lipid component of LS, enable LS to reach very low minimum surface tensions upon dynamic compression. However, the molecular characteristics that allow DPPC and other saturated lipids to reach very low surface tensions prevent them from rapidly readsorbing and respreading upon expansion. The inclusion of fluid, unsaturated phospholipids in LS provides better respreadability and slightly improved surfactant adsorption to the air−liquid interface but results in an increase in minimum surface tension (*2*). While the hydrophobic proteins of LS, SP-B and SP-C, represent only a small portion of LS, they are an essential component of LS and are necessary for the proper biophysical function of LS. The inclusion of SP-B and SP-C along with the phospholipid components greatly enhances surfactant adsorption, stability, and recycling of the lipid film, enabling proper respiration (*3, 4*).

An absence or a disruption of functional LS leads to the occurrence of two clinically relevant respiratory diseases: neonatal respiratory distress syndrome (nRDS) and acute respiratory distress syndrome (ARDS). nRDS arises from a deficiency of functional LS in premature infants due to a lack of mature alveolar type II cells in the epithelial lining of the lungs and is a leading cause of infant mortality (*1*). ARDS, on the other hand, is a more complex disorder than nRDS, resulting from multiple pulmonary and nonpulmonary causes and occurs in both children and adults. While ARDS patients initially exhibit symptoms associated with the underlying disorder, they eventually display symptoms associated with respiratory failure due to inactivation or alterations of the native LS pool. Without properly functioning LS in either nRDS or ARDS, lung compliance is reduced, and respiration is greatly impaired, ultimately resulting in alveolar collapse and suffocation without treatment.

Currently, there is no efficacious treatment for ARDS; however, nRDS is routinely treated by the administration of

† This work was supported by the National Institutes of Health (Grant 2 R01 HL67984) and the National Science Foundation (Grant BES-0101195).

* To whom correspondence should be addressed. Tel.: (650) 721-1151. Fax: (650) 723-9801. E-mail: aebarron@stanford.edu.

‡ Northwestern University.

§ Stanford University.

[1] Abbreviations: FM, fluorescence microscopy; LS, lung surfactant; LWSB, Langmuir−Wilhelmy surface balance; PBS, pulsating bubble surfactometer; SP-C, surfactant protein C; LE, liquid expanded; LC, liquid condensed; SRT, surfactant replacement therapy; γ, surface tension; γ_{ads}, adsorption surface tension; γ_{max}, maximum surface tension; γ_{min}, minimum surface tension.

10.1021/bi7021975 CCC: $40.75
Published on Web 01/16/2008

exogenous surfactant preparations into the lungs of premature infants. There are two main categories of exogenous surfactant replacement therapies (SRTs) currently used in the treatment of nRDS: synthetic formulations and natural, animal-derived formulations. Synthetic surfactants are protein-free formulations comprised of synthetic phospholipids and surface-active additives, while natural surfactants consist of surfactant extracted from animal lungs by lavage or isolated from homogenized lung tissue. Natural surfactants show significantly improved efficacy over synthetic surfactants, likely due to the presence of the hydrophobic proteins SP-B and SP-C (*5*). Despite the good efficacy of natural surfactants, there are some drawbacks associated with their use (*6*). Because natural surfactants are extracted from animal lungs, there is a possibility of cross-species transfer of antigenic or infectious agents as well as high costs and batch-to-batch variability (*7*−*10*). Therefore, there has been increasing interest in the development of a third category of SRT: biomimetic SRTs that utilize an entirely synthetic surfactant containing an accurate mimic of the hydrophobic protein portion of LS, which functions as well as the natural material while eliminating the concerns associated with animal-derived surfactants. The developments of lucinactant (Surfaxin), Venticute, and SP-C33 have shown promise as efficacious biomimetic SRTs; however, these novel surfactants are not yet clinically available; therefore, there still remains a tremendous opportunity for innovation in the development of LS replacements that are increasingly efficacious, cost-effective, and provide a long therapeutic window for the treatment of lung disorders (*11*−*13*).

SP-C is the smaller of the two hydrophobic LS proteins, at just 35 monomers in length, and is the only surfactant protein that is exclusively expressed in the lungs, lacking any known homologous proteins (*14*, *15*). The three-dimensional structure of human SP-C has been determined by 2-D NMR in an apolar solvent. SP-C is predominantly helical with an α-helix ∼37 Å long, comprised of residues 9−34 (*16*). Within this region, residues 13−28 comprise a 23 Å long, valyl-rich stretch of hydrophobic amino acids that closely matches the alkyl chain length of a DPPC bilayer. Polarized FT-IR spectroscopic studies have shown that the SP-C α-helix orients in a transbilayer orientation in a lipid bilayer, where the helical region interacts with lipid acyl chains (*17*). Two adjacent positively charged residues, lysine and arginine, at positions 11 and 12 interact with the anionic phospholipid head groups and promote surfactant protein binding to the monolayer or bilayer by ionic interactions (*18*). In human SP-C, cysteine residues at positions 5 and 6 are post-translationally modified with palmitoyl groups and are thought to be important; however, the extent of importance has been debated in the literature (*19*−*23*). In LS films, SP-C promotes phospholipid insertion into the air−liquid interface and thereby enhances the rate of lipid adsorption as well as the respreading of the alveolar film upon inhalation (*21*, *22*, *24*, *25*). The presence of SP-C has also been shown to lower, to some extent, the minimum surface tension of various lipids, to stabilize the surfactant film upon compression, and to greatly increase the surface viscosity at low surface tensions (*21*, *26*).

Because of its large number of nonpolar residues (>70%) and the two palmitoyl chains, SP-C is the most hydrophobic naturally occurring mammalian protein known (*1*). SP-C's extreme hydrophobicity coupled with its unstable secondary structure makes working with the natural protein extraordinarily difficult (*27*−*29*). This difficulty has led to the development of synthetic and recombinant analogues of SP-C to reproduce the biophysical behavior of the natural protein while minimizing the tendency for aggregation or misfolding (*30*−*32*). These analogues have offered many insights concerning the structure−activity relationships of SP-C, and researchers have identified several biomimetic polypeptide candidates for use with phospholipids to treat RDS (*33*). Despite the advantages of these synthetic and recombinant SP-C peptide mimics over the native protein, these mimics still have inherent difficulties associated with them such as being difficult to synthesize in appreciable yield, arduous purification, and marginal stability.

Recent work in our laboratory has been aimed at the development of a new category of synthetic surfactant protein mimics utilizing poly-N-substituted glycines or peptoids (*34*, *35*). Peptoids have a close structural similarity to peptides but have their side chains appended to the amide nitrogens rather than to the α-carbons. This feature renders peptoids essentially invulnerable to protease degradation, making them more biostable than peptides (*36*). Despite the achirality of the N-substituted glycine backbone and its lack of hydrogen bond donors, peptoids are able to adopt extraordinarily stable chiral helices when substituted with α-chiral, sterically bulky side chains (*37*−*39*). This ability to form stable helices makes peptoids an excellent candidate for the mimicry of bioactive molecules that rely on helical structure for proper function, such as the hydrophobic proteins of LS.

A peptoid-based mimic of SP-C with a biomimetic sequence of side chains and a longitudinally amphipathic helical secondary structure was shown to mimic many of the essential biophysical properties of SP-C when combined with a synthetic phospholipid formulation (*34*). The peptoid-based surfactant formulation was able to reach a low equilibrium surface tension and to reduce and control surface tension as a function of surface area as observed by pulsating bubble surfactometry. The biomimetic formulation also exhibited a film-phase behavior and film morphology similar to that of a formulation containing a modified SP-C peptide analogue. Here, we expand upon our previous work by investigating the biophysical behavior of several peptoid-based mimics of SP-C by systematically varying the length and chemistry of the helical hydrophobic region, which is critical to the function of the natural protein (*40*). We created and characterized two classes of mimics containing either α-chiral, aromatic-based or α-chiral, aliphatic-based helices of either 8, 11, or 14 residues in length, to determine the side chain preference and the optimal helical length of a peptoid-based mimic of SP-C. Our findings show that the incorporation of a rigid aromatic helix in a peptoid mimic of SP-C provides surface activity superior to a more biomimetic aliphatic helix, indicating that it is more important to capture the extreme hydrophobicity and highly helical structure of SP-C rather than its exact side chain chemistry. We also observe an improvement of surface activity corresponding to a longer helical length, suggesting that the optimal surface activity of these SP-C mimics is dependent on the presence of a helical hydrophobic C-terminus that is 14 *N*spe monomers in length (∼28 Å).

Table 1: Peptide and Peptoid Sequences

Molecule	Sequence/Structure
SP-C_{ff}	FGIPFFPVHLKRLLILLLLLLLLILLLILGALLMGL
Mimic 1-n n = 8, 11, 14	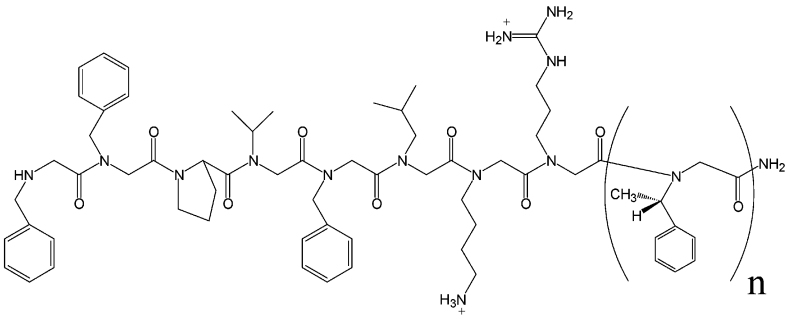
Mimic 2-n n = 8, 11, 14	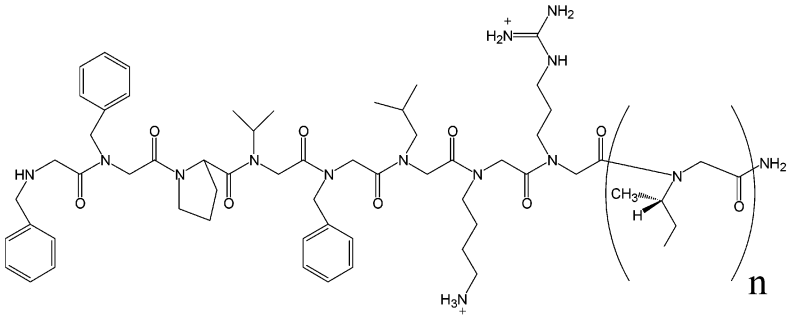

MATERIALS AND METHODS

Materials. Peptide and peptoid synthesis reagents were purchased from Applied Biosystems (Foster City, CA) and Sigma-Aldrich (Milwaukee, WI). Fmoc-protected amino acids, resins, and di-tert-butyl dicarbonate were purchased from NovaBiochem (San Diego, CA). The 2,2,5,7,8-pentamethylchroman-6-sulfonyl chloride (PMC) protecting group was purchased from Omega Chemical (Quebec, Canada). The primary amines and palmitic acid (PA) were purchased from Sigma-Aldrich in the highest purity available. All organic solvents used for sample synthesis, purification, and preparation were HPLC-grade or better and were purchased from Fisher Scientific (Pittsburgh, PA). The synthetic phospholipids DPPC and POPG were purchased from Avanti Polar Lipids (Alabaster, AL) and were used as received. Texas-Red1,2-dihexadecanoyl-*sn*-glycero-3-phosphoethanolamine triethylammonium salt (TR-DHPE) was purchased from Molecular Probes (Eugene, OR).

Protein Design and Synthesis. Because of SP-C's extreme hydrophobicity and strong tendency to misfold and aggregate in the absence of phospholipids, we synthesized a peptide analogue, SP-C_{Lff}, in which all valine residues in positions 13−28 were replaced with leucines and the palmitoylcysteines at positions 5 and 6 were replaced by phenylalanine residues (Table 1) (*28*, *29*, *31*, *41*). This peptide analogue is based upon the SP-C analogues developed by Nilsson et al. in which leucine residues replace the transmembrane valine residues for improved solubility and stability of the α-helical secondary structure and the recombinant mimic developed by Ikegami and Jobe where the palmitoylcysteines were replaced by phenylalanines (*31*, *32*). Both peptide mimics were shown to have favorable surface activity when combined with a biomimetic phospholipid formulation.

SP-C_{Lff} was synthesized on a 0.25 mmol scale on an Applied Biosystems 433A automated peptide synthesizer, using standard Fmoc chemistry, and a prederivatized Wang-Leu resin. Cleavage and deprotection of the peptide resin was carried out by mixing it with aqueous 90% TFA and necessary scavengers for 2 h. The reaction mixture was then immediately filtered, diluted with isopropyl alcohol and water, frozen, and lyophilized to yield the crude peptide. The crude material was then redissolved in isopropyl alcohol.

The crude SP-C peptide was purified on a Waters reversed-phase HPLC system (Waters Corp., Milford, MA) with a Vydac C4 column (Vydac, Hesperia, CA) with a linear gradient of 25−100% solvent B in solvent A over 50 min (solvent A is 0.1% TFA in water and solvent B is 0.1% TFA in isopropyl alcohol). The resulting fractions were lyophilized to remove excess solvent and trace amounts of TFA. The dried fractions were then reconstituted in TFA-free isopropyl alcohol and analyzed by analytical HPLC. Fractions, which were determined to be pure, were then combined and lyophilized at least twice more. The final purity of the peptide was determined by reversed-phase HPLC to be >97%. Electrospray mass spectrometry confirmed the molar mass of the purified peptide to match that of the desired compound (3924 Da).

Peptoid Synthesis. The peptoid-based SP-C mimics shown in Table 1 were synthesized on an automated 433A ABI Peptide Synthesizer (Foster City, CA) on a solid support (Rink amide resin), following a two-step submonomer

method as described by Zuckermann et al. (*42*). Briefly, synthesis was carried out on 0.25 mmol of Rink amide resin (Novabiochem, San Diego, CA). After the removal of the first Fmoc protecting group from the resin with 20% piperidine in *N*,*N*-dimethylformamide (DMF) and rinsing of the resin with DMF, the monomer addition cycle was performed by first acetylating the resin with the addition of 1.2 M bromoacetic acid in DMF, followed by *N*,*N*-diisopropyl carbodiimide in DMF. The acetylation step was carried out for 45 min, and then the resin was washed with DMF. The resin-bound halogen was then displaced by 1.0 M primary amine submonomer in *N*-methylpyrrolidinone (NMP), which was added to the resin and allowed to react for 90 min. The two-step cycle was repeated until the desired length and sequence of the peptoid was obtained, except for the addition of the *N*lys, *N*arg, and proline residues. The displacement step for the PMC-protected *N*arg and Boc-protected *N*lys residues was extended to 120 min, while for the addition of the proline residue, a PyBrop activating system was employed. After the proline addition, the Fmoc group was removed with piperidine as before, and the peptoid cycle was continued.

Peptoid oligomers were cleaved from the resin and deprotected with 90% TFA along with necessary scavengers for either 15 min for mimics 1−*n* or 40 min for mimics 2−*n* (Table 1). The crude products were then purified by preparative HPLC on a Waters system with a Vydac C4 column and a linear gradient of 30−80% solvent C in solvent A over 70 min (solvent C is 0.1% TFA in isopropyl alcohol/acetonitrile, 1:1). The final purity of the peptoids was confirmed by reversed-phase HPLC to be >97%. Electrospray mass spectrometry was used to confirm the correct molar masses.

Circular Dichroism (CD) Spectroscopy. CD measurements were performed on a Jasco model 715 spectropolarimeter (Easton, MD). Stock solutions for dilution to appropriate concentrations for CD were made immediately before analysis in tared 4.0 mL vials by precise weighing of added solvent and at least 2 mg of lyophilized peptoid powder, to produce a sample of accurately known concentration. The stock solutions were then diluted to CD sample concentration (∼60 μM). CD spectra were acquired in a quartz cylindrical cell (Hellma model 121-QS, Forest Hills, NY) with a path length of 0.02 cm, employing a scan rate of 100 nm/min. CD spectra reported here represent the average of 40 successive spectral accumulations. Data are expressed in terms of per-residue molar ellipticity (deg cm^2/dmol), as calculated per mol of amide groups present and normalized by the molar concentration of peptoid. The α-helical content of the SP-C peptide, SP-C$_{Lff}$, was estimated using the graphical interface DICHROWEB employing the SELCON3 analysis program (*43*−*45*). Repeat measurements were conducted approximately 2 months later, and no significant changes in CD spectra were observed.

Langmuir−*Wilhelmy Surface Balance (LWSB) and Fluorescence Microscopy (FM).* Surface pressure (Π)−area (*A*) isotherms were obtained using a home-built Langmuir−Wilhelmy surface balance as previously described (*35*). For each experiment, the trough was filled with a buffered subphase (0.15 M NaCl, 5 mM $CaCl_2$, and 10 mM HEPES at pH 6.90) and heated to either 25 or 37 °C. A Wilhelmy surface balance (Reigler and Kirstein, Berlin, Germany) was then calibrated and used to monitor the surface pressure as the area of the trough was either expanded or compressed. The surfactant material in an organic solution was spread at the air−liquid interface using a syringe and allowed to equilibrate for 10 min. The barriers were then compressed at a rate of 30 mm/min. Determination of the surfactant respreadability was also performed for each formulation (*1*, *46*).

To obtain fluorescence microscopic images, a Nikon MM40 compact microscope stand with a 100 W mercury lamp (Tokyo, Japan) was used in conjunction with the Langmuir trough. Fluorescence was detected by a Dage-MTI three-chip color camera (Dage-MTI, Michigan City, IN) in conjunction with a generation II intensifier (Fryer, Huntley, IL). Samples were spiked with 0.5 mol % of a fluorescently labeled lipid, TR-DHPE, for detection. Previous studies have shown that inclusion of the labeled lipid at this concentration did not alter the surfactant film morphology (*47*). Experiments were performed on an aqueous buffered subphase at 37 °C with a barrier speed of 5 mm/min. The images were resized and enhanced in contrast and brightness within reasonable limits to make the features discernible for the purpose of display when warranted (*48*).

Pulsating Bubble Surfactometer (PBS). Static and dynamic characterization of surfactant film properties were performed on a modified PBS (General Transco, Largo, FL) as described by Seurynck et al. in which an imaging system is employed to accurately track bubble size and shape throughout the experiment (*49*). Briefly, the lipid mixture (DPPC/POPG/PA, 68:22:9 (by wt)) was dissolved in chloroform/methanol (3:1) and spiked with 1.6 mol % SP-C mimic, analogous to 10 wt % SP-C peptide (*50*). The samples were prepared in Eppendorf tubes, dried under vacuum, and resuspended at room temperature in an aqueous buffer solution (0.15 M NaCl, 5 mM $CaCl_2$, and 10 mM HEPES at pH 6.90) to a phospholipid concentration of 1.0 mg/mL. Samples were then mixed with a pipet 20 times, sonicated with a probe sonicator for 15 s twice, and then mixed again 20 times with a pipet. Samples were then loaded into the sample chamber using a modified leak-free methodology (*51*). The sample chamber was placed in the PBS at a temperature of 37 °C. A bubble with a radius of 0.4 mm was then formed, and an imaging acquisition system was used to determine the bubble size. The trans-film bubble pressure was recorded as a function of time while holding bubble radius static for 20 min during static adsorption experiments. Dynamic measurements of surface tension as a function of bubble surface area were subsequently collected by cycling the bubble radius between approximately 0.4 and 0.55 mm at an oscillation frequency of 20 cycles/min for 10 min.

RESULTS AND DISCUSSION

Peptoid Design and Rationale. Our previous work with a peptoid-based mimic of SP-C utilized similar design strategies to those that have been employed in the design of peptide-based SP-C analogues. Specifically, the peptoid mimic was designed to emulate essential features of SP-C, including extreme hydrophobicity, patterning of hydrophobic and polar residues, and a highly helical structure. The peptoid-based mimic of SP-C used in those studies contained

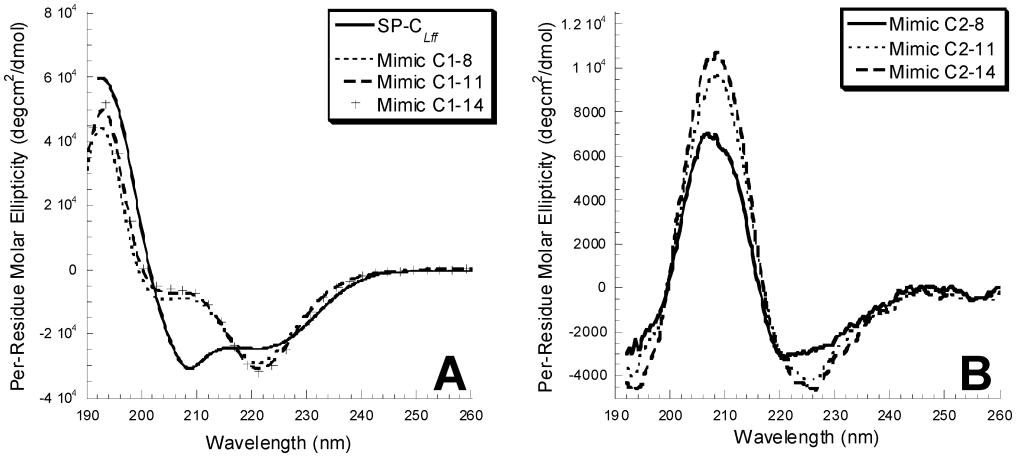

FIGURE 1: (A) CD spectra of the SP-C_{Lff} peptide as well as of the varied-length *N*spe-based peptoid SP-C mimics (mimics 1−8, 1−11, and 1−14), showing qualitatively similar features characteristic of peptide and peptoid helices, respectively. (B) CD spectra of the varied-length *N*ssb-based peptoid SP-C mimics (mimics 2−8, 2−11, and 2−14) displaying the characteristic features of polyproline type I helices. Spectra were acquired in methanol at a concentration of ~60 μM, at room temperature.

a helical hydrophobic stretch composed of 14 α-chiral aromatic (*N*spe) monomers and an achiral amino-terminal stretch composed of 8 peptoid monomers with side chains analogous to those present in positions 5−12 of human SP-C. This mimic was shown to yield a helical secondary structure similar to that of an SP-C peptide as well as its surface activity when combined with a biomimetic phospholipid formulation despite the presence of a hydrophobic aromatic helix (*34*). This suggested that the critical features of SP-C are its longitudinally amphiphathicity and highly helical structure rather than the exact side chain chemistry. However, it was not known if the incorporation of a more biomimetic helical region utilizing aliphatic side chains, which are more similar to valine side chains that predominate mammalian SP-C, in a peptoid mimic would have a beneficial impact on surface activity.

In this study, we investigated the effects of varying both the side chain chemistry and the length of the hydrophobic helical region of a SP-C peptoid mimic. Two main categories of SP-C mimics were studied: those utilizing α-chiral aromatic side chains (*N*spe) in the helical region (mimics 1−*n*) and those utilizing α-chiral aliphatic side chains (*N*ssb) in the helical region (mimics 2−*n*). The length of the helical region of the mimics was also systematically varied to determine the effect of helix length on surface activity. The side chains and the sequences of the various peptoid mimics studied are shown in Table 1.

Sequences composed of *N*spe residues form extremely stable helices, an important feature in mimicking SP-C; however, the aromatic side chains have a very different structure than that present in the helix of mammalian SP-C, which is entirely aliphatic, consisting of valine, leucine, and isoleucine residues. Therefore, we investigated peptoid mimics incorporating more biomimetic side chains (*N*ssb) that also form stable right-handed helices of the same class (*52*). While both classes of mimics form stable right-handed helices with three residues per turn, the α-chiral aromatic side chains of *N*spe are able to adopt a tighter, more rigid secondary structure with a helical pitch of ~6.0 Å as opposed to ~6.7 Å per turn for aliphatic-based peptoid helices. Both classes of mimics were studied to gain greater insight into whether the helical stability or side chain biomimicry has a greater impact on its surface activity in a lipid environment. In addition to side chain chemistry, the specific length of the hydrophobic helical region was also investigated by varying the number of α-chiral helix forming peptoid residues in this region to determine the minimal helical length of a SP-C peptoid mimic. Both classes of mimics were varied by approximately one turn of the helix by incorporating 8, 11, and 14 helix inducing residues. A distinct advantage of both classes of peptoid mimics over the natural SP-C protein or peptide SP-C analogues is the absence of any observable aggregation over time in the absence of phospholipids.

Secondary Structure. CD was used to characterize and compare the secondary structure of the SP-C peptide and the various peptoid-based SP-C mimics. It has been previously shown that both a non-palmitoylated human-identical SP-C peptide and a dipalmitolyated peptide mimic of SP-C form predominantly α-helical structures as observed by CD (*31*, *53*−*55*). The highly helical nature of SP-C has been shown to be essential for its surfactant activity (*40*). CD spectra of the modified SP-C peptide, as well as that of the peptoid-based SP-C mimics, are displayed in Figure 1. SP-C_{Lff} displays CD spectral features that are characteristic of an α-helix, consistent with previously published results, having an estimated α-helical content of 74% (*54*). The peptoid-based SP-C mimics containing α-chiral aromatic residues (*N*spe) exhibit CD features that are similar to the SP-C peptide, with each showing an intense maximum at λ = ~192 nm and double minima at λ = ~205 and ~220 nm (Figure 1A). These spectral features are characteristic signatures of a helical peptoid structure in oligomers of this class, with highly ordered backbone amide bonds (*38*). The intensities of the helical spectrum for the aromatic-based mimics are very similar, with mimic 1−14 (22mer) displaying the strongest intensity and that of mimics 1−11 (19mer) and 1−8 (16mer) being only slightly weaker. The decrease in intensity of the helical signal coincides with a reduction in the length of the helical hydrophobic stretch of the mimics, similar to what has been observed with other peptoid oligomers (*56*).

A different type of CD spectrum was observed for the peptoid SP-C mimics with α-chiral aliphatic residues (*N*ssb) in the helical region (Figure 1B). These peptoid mimics

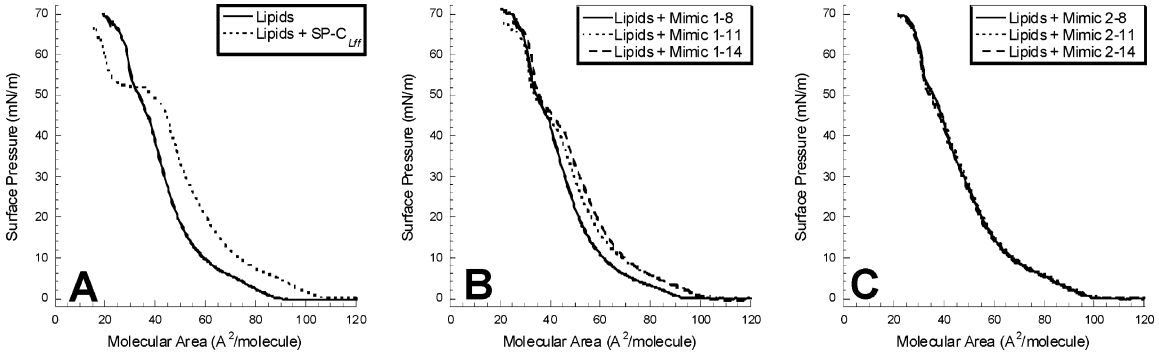

FIGURE 2: LWSB studies at 25 °C (A) Π−A isotherms obtained for DPPC/POPG/PA (68:22:9, by wt) alone and with 1.6 mol % SP-C$_{Lff}$ peptide. (B) 1.6 mol % *N*spe-based peptoids (mimics 1−8, 1−11, and 1−14). (C) 1.6 mol % *N*ssb-based peptoids (mimics 2−8, 2−11, and 2−14). Isotherms were collected on a buffered subphase (150 mM NaCl, 10 mM HEPES, 5 mM $CaCl_2$, pH 6.90).

exhibit CD spectral features that are similar to those characteristic of a polyproline type I peptide helix, but blue-shifted, which is characteristic of peptoids of this class (*52*, *57*). Mimic 2−14 (22mer) displays the strongest CD intensity, while mimics 2−11 (19mer) and 2−8 (16mer) display progressively weaker CD signal intensities, similar to the aromatic-based mimics. Despite differences in the type of CD spectra observed for the various compounds, all of the SP-C mimics are shown to be helical and structured, satisfying one of the structural criteria, helicity, believed to be of importance for the surface activity of SP-C (*40*).

LWSB Studies. To determine the effect of the *N*spe- and *N*ssb-based SP-C peptoid mimics on the monolayer-phase behavior of the lipid formulation, the mimics were combined at 1.6 mol % with an optimized lipid formulation comprised of DPPC/POPG/PA (68:22:9, by wt). This formulation has been shown to closely mimic the behaviors of the lipid portion of LS (*50*, *58*). While PA does not constitute a significant portion of natural LS, it has been successfully included in effective clinical preparations and is widely used for both in vitro and in vivo testing. The resulting formulations were studied on the LWSB as previously described. The Π−*A* isotherms for the lipid formulation alone and with SP-C$_{Lff}$ at 25 °C are shown in Figure 2A, and the *N*spe- and *N*ssb-based peptoid formulations are shown in Figure 2B,C, respectively.

The Π−*A* isotherm observed for lipids alone has a liftoff point (defined as the *A* where Π first increases) of ∼90 Å^2/molecule. The slope of the Π−*A* isotherm is relatively small up to a Π value of ∼10 mN/m, indicating a high compressibility typical of the LE phase. As the surface layer is further compressed from 10 to ∼44 mN/m, the slope of the isotherm increases, indicating a less compressible film and consistent with the formation of condensed domains of DPPC that are cocrystallizing with PA and coexisting with the LE phase (*59*, *60*). Further compression of the lipid film leads to a slight kink in the Π−*A* isotherm at ∼44 mN/m and eventually a collapse pressure of ∼70 mN/m. The addition of SP-C$_{Lff}$ to the lipid mixture shifts the liftoff point to a greater molecular area (∼108 Å^2/molecule vs ∼90 Å^2/molecule), indicating increased surface activity and an earlier transition to a LE state due to the presence of the SP-C peptide at the air−liquid interface. At low surface pressure, the Π−*A* isotherm is similar to lipids alone, only shifted toward a higher molecular area. However, further compression results in the occurrence of a dramatic plateau region beginning at Π = ∼48 mN/m. The isotherm plateau is also observed for natural LS and is theorized to indicate a phase transition in the lipid film or the reversible removal of lipids and proteins from the monolayer, forming a surface-associated reservoir near the interface (*61*). The presence of such a surfactant reservoir offers an explanation as to how the SP-C protein is able to interact with lipids to provide low surface tension upon compression and also to respread rapidly on expansion (*61*, *62*). A dramatic increase in surface viscosity was also observed for SP-C containing films at or above the plateau and is thought to help minimize the loss of surfactant material from the alveoli at low surface tensions and is also partially responsible for the high collapse pressure associated with LS (*26*). Further compression of the SP-C containing formulation leads to a high collapse pressure of ∼70 mN/m.

The addition of mimic 1−8 to the lipid formulation results in a Π−*A* profile very similar to that of the lipid mixture alone, with a very slight increase in liftoff to *A* = ∼95 Å^2/molecule as compared to ∼90 Å^2/molecule for the lipid system and a similar kink in the isotherm at Π = ∼44 mN/m (Figure 2B). Increasing the helical length from 8 to 11 *N*spe residues results in an additional increase in molecular area liftoff of ∼105 Å^2/molecule and a slightly more pronounced kink/plateau in the isotherm beginning at Π = ∼42 mN/m. A further increase of the helical length to 14 residues, mimic 1−14, results in a similar liftoff as the formulation containing mimic 1−11 and with a Π−*A* isotherm that overlays mimic 1−11 up to a Π value of ∼10 mN/m. Further compression of the mimic 1−14 system past Π = ∼10 mN/m results in a surface layer that is slightly less compressible than the mimic 1−11 system. At Π = ∼42 mN/m, a biomimetic plateau is present in the mimic 1−14 system, which occurs at the same Π value as the mimic 1−11 system but is slightly more pronounced (although not as prominent as in the SP-C peptide system). These Π−*A* features make the formulation containing mimic 1−14 the closest in monolayer-phase behavior to the SP-C peptide system. Given SP-C's helical length, orientation in a lipid environment, and ability to catalyze the formation of lipid bilayers, it is reasonable that mimic 1−14, which most closely approximates the helical length of SP-C, should have the most similar monolayer-phase behavior as the SP-C peptide (*63*, *64*).

The addition of mimic 2−8 to the lipid formulation results in an increase in the liftoff to ∼100 Å^2/molecule with a very slight kink in the isotherm that is similar to the lipid system (Figure 2C). Unlike the *N*spe-based mimics, further lengthening of the hydrophobic region does not improve the surface

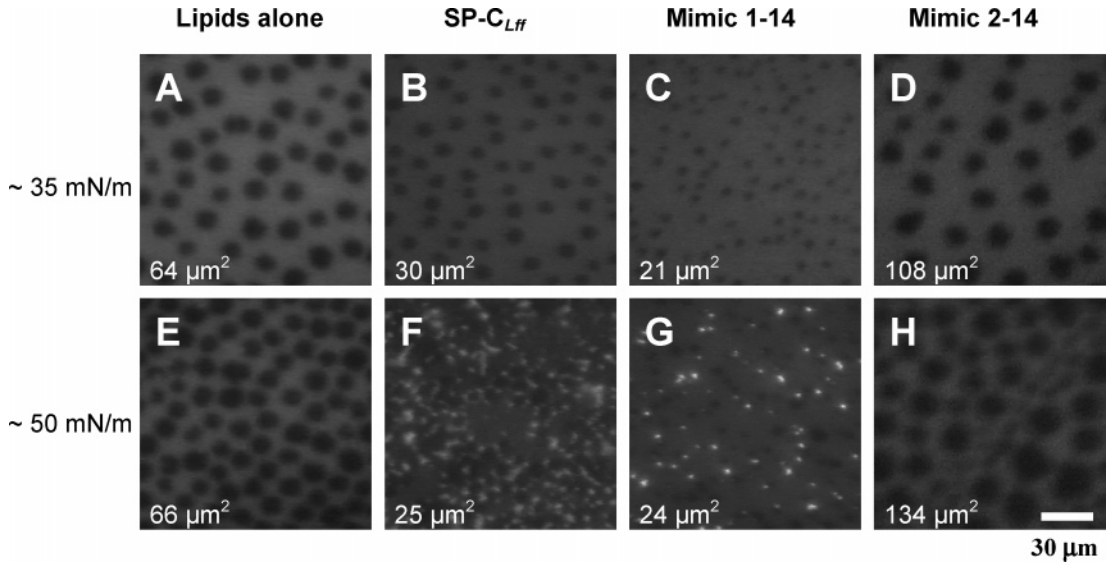

FIGURE 3: FM micrographs at 37 °C corresponding to Π values of ∼35 and ∼50 mN/m for DPPC/POPG/PA (68:22:9, by wt) alone (A and E), with 1.6 mol % SP-C$_{Lff}$ peptide (B and F), with 1.6 mol % mimic 1−14 (C and G), and with 1.6 mol % mimic 2−14 (D and H). Average size of the dark LC domains for each film is indicated in the lower left of each panel.

activity of the surfactant for the *N*ssb-based mimics. The addition of either mimic 2−11 or mimic 2−14 to the lipid system results in a similar liftoff of $A = \sim 100$ Å^2/molecule and just a slight kink in the isotherm at $\Pi = \sim 48$ mN/m. The isotherms for all of the *N*ssb-based mimics essentially overlay one another, suggesting a relative insensitivity to helical length in relation to surface activity and only a minor alteration of surface activity and lipid organization due to the presence of this class of mimics. It is possible that the less rigid *N*ssb-based helices are less efficient in forming the requisite three-dimensional structures that normally coincide with an extended plateau region in the Π−*A* isotherm of LS.

To determine the respreadability of the surfactant films, the surface layers were compressed as before except that compression was continued approximately 10 Å/molecule past collapse. The surface films were then expanded and compressed to the same point. By comparing the ratio of the two collapse plateau regions of the Π−*A* isotherms, the relative respreadability was determined for each preparation (*1*, *46*). All surfactants with added peptoid-based SP-C analogues had similar respreadabilities, ∼82%, which were superior to the lipids alone, ∼73% (data not shown).

FM Imaging of Film Morphology. To gain more detailed information about the interactions of the lipids and the SP-C mimics, the surface-phase morphology of the surfactant films with and without SP-C$_{Lff}$ and the longer length peptoid mimics, mimics 1−14 and 2−14, were investigated. Figure 3 displays the FM images of the surfactant films at $\Pi = \sim 35$ mN/m (panels A−D) and at $\Pi = \sim 50$ mN/m (panels E−H). The pure lipid system displays nucleation of the dark liquid condensed (LC) domains beginning at $\Pi = \sim 20$ mN/m, and a continuous growth of larger, circular-shaped LC domains with increased compression (Figure 3A,E). The coexistence of both LE and LC domains is a common feature of most LS formulations. This phase coexistence is important in controlling surface viscosity and film mechanical properties, promoting high collapse pressure. At a Π value of ∼35 mN/m, the lipid film exhibits circular LC domains of ∼64 μm^2 that occupy ∼23% of the total film area. This is similar to the morphology observed at $\Pi = \sim 50$ mN/m but with the appearance of a few small vesicles (bright spots) scattered throughout the film at the increased Π value (Figure 3E).

At ∼35 mN/m, the film containing the SP-C peptide has a morphology similar to the lipids alone with the appearance of circular LC domains; however, the LC domains are significantly smaller, ∼30 μm^2, and occupy approximately 15% of the film area. The LC domains for mimic 1−14 are also smaller in size than the lipids alone, ∼21 μm^2, and occupy only 10% of the film area (Figure 3C). Adding mimic 2−14 to the lipid film surprisingly results in larger LC domains, ∼108 μm^2, that occupy roughly 23% of the film area (Figure 3D). Increasing the surface pressure to ∼50 mN/m results in varied film morphology for the different surfactant formulations. The addition of SP-C$_{Lff}$ to the lipid film results in the nucleation of numerous bright vesicle domains or likely three-dimensional protrusions throughout the film (Figure 3F). The domains for the SP-C$_{Lff}$ containing film remain approximately the same size and area as at the lower pressure. The lipid film containing mimic 1−14 shows a similar film morphology and LC domain size to that of the SP-C$_{Lff}$ film, although with less vesicle formation (Figure 3G). Interestingly, the addition of mimic 2−14 to the lipid film results in a film morphology that is very similar to the lipids-alone film with minimal vesicle formation (Figure 3H). The greater extent of biomimicry of the *N*spe-based formulation versus the *N*ssb-based formulation is consistent with the results of the LWSB experiments.

Adsorption. One of the biophysical characteristics that is important to mimic with an LS replacement is the ability of natural LS to adsorb rapidly to an air−liquid interface, forming a surface-active layer (*1*, *33*). The adsorption kinetics of the lipid mixture alone, and with the addition of 1.6 mol % SP-C mimics, was characterized with a modified PBS run in static mode with a bubble radius of approximately 0.40 mm at 37 °C. Figure 4 displays the adsorption surface tension (γ_{ads}) as a function of time for the various lipid formulations. In the absence of SP-C mimics, the lipid mixture displays very slow surface adsorption and fails to reach a γ_{ads} value of lower than 57 mN/m even after 20 min of static adsorption

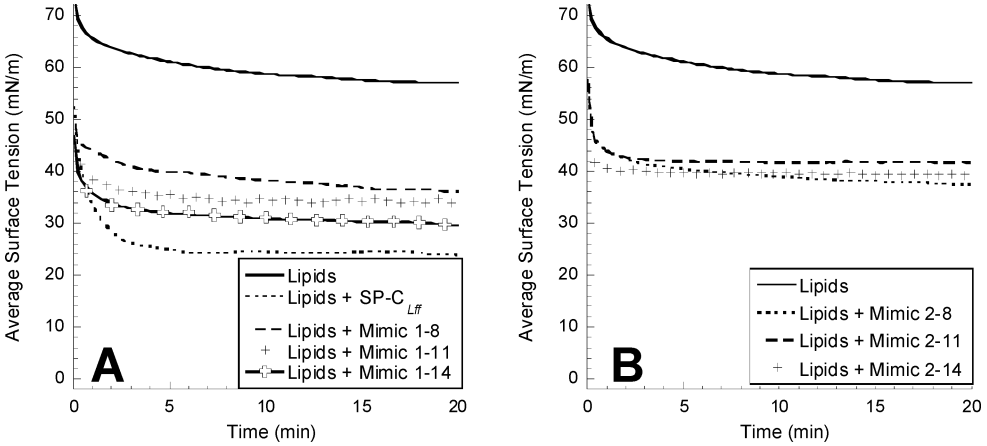

FIGURE 4: Static PBS results displaying surface tension as a function of time. Measurements were taken at a bulk surfactant concentration of 1 mg/mL lipids and at 37 °C. (A) Lipid mixture alone and with 1.6 mol % SP-C$_{Lff}$ and *N*spe-based peptoids (mimics 1−8, 1−11, and 1−14). (B) Lipid mixture alone and with 1.6 mol % *N*ssb-based peptoids (mimics 2−8, 2−11, and 2−14).

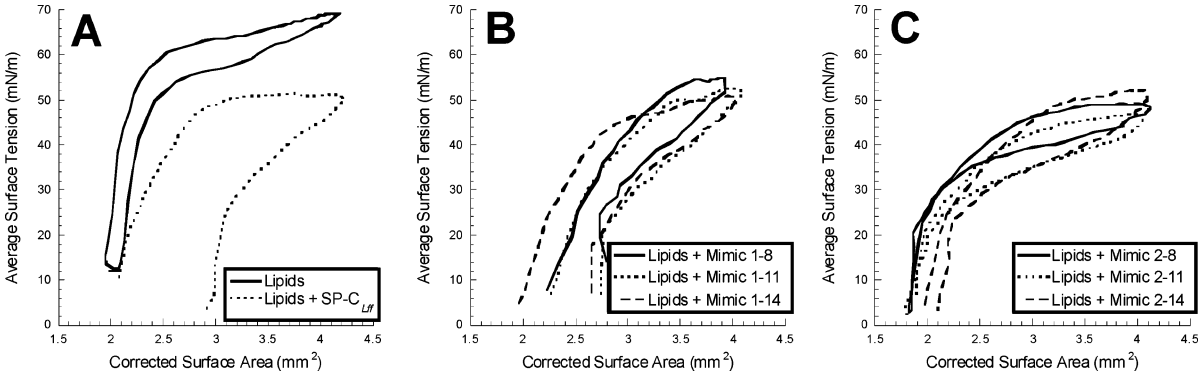

FIGURE 5: Dynamic PBS results displaying surface tension as a function of surface area at an oscillation frequency of 20 cycles/min, after 10 min of initial cycling. Measurements were taken at a bulk surfactant concentration of 1 mg/mL lipids and at 37 °C. (A) Lipid mixture alone and with 1.6 mol % SP-C$_{Lff}$. (B) Lipid mixtures with 1.6 mol % *N*spe-based peptoids (mimics 1−8, 1−11, and 1−14). (C) Lipid mixtures with 1.6 mol % *N*ssb-based peptoids (mimics 2−8, 2−11, and 2−14).

(natural, animal-derived LS reaches $\gamma_{ads} = \sim 20-25$ mN/m within a few seconds) (*65*). The addition of SP-C$_{Lff}$ to the lipid formulation significantly accelerates the kinetics of lipid adsorption to the interface, allowing the film to reach a γ_{ads} value of approximately 30 mN/m in just over 1 min, with γ_{ads} dropping below 25 mN/m after 5 min. The addition of the shorter-length *N*spe-based mimic, mimic 1−8, to the lipid formulation similarly results in accelerated adsorption kinetics over lipids alone, but the rate is slower, and this formulation is only able to reach a γ_{ads} value of ∼37 mN/m after 20 min. The addition of mimics 1−11 and 1−14 also improves the adsorption kinetics of the lipid film. An increase in adsorption kinetics is observed with increasing peptoid helix length. The formulation containing mimic 1−14 is able to reach a γ_{ads} value of ∼30 mN/m after 20 min and is most similar to the formulation containing the SP-C peptide but still does not perform as well. The inclusion of mimics 2−*n* in the lipid formulation also improves the adsorption to the interface over lipids alone; however, to a much lesser extent than the *N*spe-based mimics and, unlike Mimics 1−*n*, no improvement in adsorption is observed with increasing helical length. The *N*ssb-based mimic formulations only reach a γ_{ads} value of ∼40 mN/m after 20 min.

On the basis of these results, we conclude that the kinetic adsorption behavior of the surfactant is enhanced with the addition of either class of peptoid mimics to the lipid formulation. However, the aromatic-based mimics are able to adsorb to lower surface tensions than the aliphatic-based mimics, suggesting that the greater hydrophobicity and structural rigidity of the aromatic helix is better able to facilitate surfactant adsorption to the air−liquid interface. An improvement in adsorption corresponding to greater helical length is also observed with the aromatic-based mimics, suggesting that a minimum helical length of 14 *N*spe residues is required to mimic the adsorption behavior of SP-C$_{Lff}$.

Dynamic Cycling. To investigate the effectiveness of the peptoid-based SP-C mimic formulations to reduce and control surface tension as a function of surface area, PBS experiments were performed in a dynamic mode at an oscillation frequency of 20 cycles/min and ∼50% reduction in surface area. Features that are important in the compression−expansion loop for biomimetic surfactant film behavior include: (i) the ability to reach a very low surface tension with a small percentage of compression, (ii) the ability to respread rapidly, and (iii) the ability to control surface tension as a function of bubble surface area with the lowest minimum surface tension (γ_{min}) and lowest maximum surface tension (γ_{max}) possible (*1*, *33*). Figure 5 displays the surface tension as a function of bubble surface area for lipid mixtures with and without the SP-C peptide (5A) and those containing mimics 1−*n* (Figure 5B) and mimics 2−*n* (Figure 5C). Key parameters of the dynamic compression cycles are also listed in Table 2.

Table 2: Dynamic PBS Properties[a]

formulation	γ_{max} (mN/m)	γ_{min} (mN/m)[b]	compression (%)[c]
Lipids	66.9 ± 2.12	11.6 ± 1.40	46.3 ± 3.17
lipids + SP-C_{Lff}	51.3 ± 1.75	<1	25.8 ± 2.67
lipids + mimic 1−8	55.5 ± 0.75	<1	31.7 ± 1.71
lipids + mimic 1−11	53.3 ± 0.68	<1	31.2 ± 1.54
lipids + mimic 1−14	52.9 ± 2.07	<1	33.9 ± 4.14
lipids + mimic 2−8	49.7 ± 1.47	1.39 ± 2.05	55.3 ± 2.68
lipids + mimic 2−11	48.9 ± 1.56	<1 ± 0.98	52.9 ± 3.15
lipids + mimic 2−14	51.2 ± 1.49	<1	48.2 ± 1.78

[a] Data are mean ± SD. [b] All experimental runs reached a γ_{min} value of less than 1 mN/m except for formulations comprised of lipids without any added SP-C analogue and those containing the shorter length *N*ssb-based analogues, mimics 2−8 and 2−11. [c] Compression refers to the amount of compression necessary to reach a γ value of less than 20 mN/m.

The lipid mixture, when used alone, exhibits high γ_{min} and γ_{max} values of ∼12 and ∼67 mN/m, respectively. In addition, a surface tension below 20 mN/m for the lipid formulation is only reached with a significant degree of film compression, ∼46% compression (Table 2). With these properties, this material would be inadequate as a lung surfactant replacement. The addition of SP-C_{Lff} to the lipid mixture dramatically improves the surface activity of the film relative to that of the lipids alone, as indicated by the significantly lower γ_{min} value of <1 mN/m and γ_{max} value of ∼51 mN/m (Figure 5A). The addition of SP-C_{Lff} to the lipid formulation also significantly decreases the compressibility of the surfactant, requiring much less compression, ∼26%, to reach a γ value below 20 mN/m.

The addition of mimics 1−*n* to the lipid formulation results in a surface behavior rather similar to that observed with the SP-C peptide formulation (Figure 5B). Mimics 1−8, 1−11, and 1−14 exhibit similar compression−expansion loops, all reaching a γ_{min} value of <1 mN/m upon compression. Not only is γ_{min} greatly reduced with the addition of the *N*spe-based mimics, but the amount of compression required to reach γ_{min} is also much less than for the lipids alone and is similar to the SP-C_{Lff} formulation (∼31−34% compression). Upon expansion to the maximum surface area, these formulations obtained a γ_{max} value that was also significantly lower than the lipid formulation and similar to the SP-C peptide (γ_{max} = ∼56 mN/m for mimic 1−8 and ∼53 mN/m for mimics 1−11 and 1−14). An increase in the amount of hysteresis in the compression expansion loop corresponding to increasing helical length was also observed in the aromatic mimics, which is indicative of the decreased compressibility and increased elasticity of the films containing the *N*spe-based analogues.

Compression−expansion loops obtained with lipid mixtures containing mimics 2−*n* are shown in Figure 5C. These mimics also display enhanced surface activity in comparison to the lipids-alone mixture, with a significant reduction in both maximum and minimum surface tension values (γ_{max} = ∼49−51 mN/m and γ_{min} < 1 to just over 1 mN/m). Despite the improvement over lipids alone, none of the *N*ssb-based mimics were able to replicate the surface activity of either the *N*spe-based mimics or the SP-C peptide. Specifically, all aliphatic-based formulations required significantly more compression to reach low surface tension values. Also observed was an elevated γ_{min} for the mimic 2−8 containing formulation. Although the inclusion of the *N*ssb-based mimics provides an improvement over the surface activity observed for the lipids alone, it does so to a lesser extent than the corresponding *N*spe-based mimics. The reduced surface activity of the *N*ssb-based mimics is consistent with the static measurements of surface tension versus time, which showed that the aromatic-based mimics have a superior activity as compared to the aliphatic-based mimics.

It is possible that the less rigid and slightly less hydrophobic *N*ssb-based helices are not able to associate as well with the lipid acyl chains as the *N*spe-based helices and, as a result, are not as efficient in the formation of lipid bilayers, yielding a more compressible surfactant film and a higher γ_{min} value. This hypothesis is consistent with both the LWSB and the FM studies of the peptoid-based formulations. Each of the *N*spe-based formulations contained a more pronounced plateau region than the *N*ssb-based formulations in the $\Pi-A$ isotherms, suggesting a greater structural transition at higher surface pressures. The FM studies also showed that the formulation containing the aromatic mimic, mimic 1−14, was better able to replicate the film morphology of the SP-C peptide than the aliphatic mimic, mimic 2−14, with the occurrence of bright vesicle domains also consistent with multilayer formation. These multilayer protrusions induced by the presence of SP-C have been shown to coincide with a dramatic increase in film viscosity, providing low surface tension with minimal compression while respreading rapidly on expansion (*23*, *55*, *56*, *58*).

CONCLUSION

We synthesized, designed, and characterized two classes of peptoid mimics of SP-C having either an aromatic-based or an aliphatic-based hydrophobic helix to investigate the effect of side chain biomimicry on surface activity. The length of the helical region of these mimics was also varied to determine an optimal helix length. These peptoid-based SP-C mimics preserve the longitudinally amphipathic patterning and helical secondary structure of the native SP-C molecule. The secondary structure of each mimic was determined by CD spectroscopy and found to conform to a stable helical structure with an increase in spectra intensity corresponding to increasing helical length for both classes of mimics. The peptoid mimics of SP-C were then combined with a synthetic phospholipid formulation and characterized in vitro by LWSB, FM, and PBS studies. In general, the aromatic-based peptoid mimics showed superior surface activity relative to the aliphatic-based mimics. An increase in surface activity of the aromatic-based mimics was also observed coinciding with an increase in the number of helix forming peptoid residues in the hydrophobic region of the molecule.

LWSB and FM studies confirmed that the aromatic-based mimics are able to more closely mimic the surface behavior of the SP-C peptide. The formulation containing mimic 1−14 showed an earlier liftoff, more pronounced plateau, and a much more biomimetic-phase morphology than the other peptoid-based mimic formulations and most closely replicated the SP-C peptide formulation. Static PBS adsorption studies showed that the addition of either class of peptoid mimic to a lipid formulation resulted in improved surface film adsorption kinetics over lipids alone; however, the aromatic-based peptoid mimics displayed superior adsorption

(to a lower surface tension) as compared to the aliphatic mimics with the longest helical mimic, mimic 1−14, having the most SP-C-like surface adsorption. Dynamic compression and expansion cycles on the PBS revealed that while both classes of mimics are able to reduce the γ_{max} and γ_{min} values of the lipid formulation in a similar manner as the SP-C peptide, only the aromatic-based mimics are able to significantly reduce the amount of compression required to reach γ_{min}. We also observed an increase in the amount of hysteresis in the PBS loops as the length of the helical region is increased, similar to what was observed for the adsorption experiments.

While all the aromatic-based peptoid mimics exhibit improved surface activity over lipids alone, only the longest length aromatic mimic with 14 *N*spe residues in the helical region was able to most closely replicate the surface activity of the full-length SP-C peptide. It is hypothesized that this longer length mimic with a helical region that is approximately 28 Å in length is better able to anchor in the lipid film than the truncated mimics. This is in agreement with previous studies of synthetic SP-C peptides, which showed that oligomers of varying lengths exhibited a similar activity, as long as a certain core sequence (residues 5−32) was conserved (*30*).

The specific side chain chemistry of the hydrophobic helix also significantly altered the surface activity of the peptoid mimics. All the aromatic-based mimics exhibited superior surface activity as compared to the aliphatic-based mimics as observed by LWSB, FM, and PBS. This was somewhat unexpected given that the side chains present in mammalian SP-C are closer in structure to the aliphatic mimics. We believe that this may be the case for peptoids, for two specific reasons: (i) peptoids composed of α-chiral aromatic residues adopt a tighter, more rigid helix than aliphatic-based peptoids, and this more rigid helix is necessary for modulating the surface film and (ii) the α-chiral aromatic residues used in the aromatic mimics are slightly more hydrophobic than the α-chiral aliphatic residues studied, which may facilitate better insertion into the alkyl region of the lipid film and surface activity. This suggests that the important structural feature of SP-C to mimic is its rigid hydrophobic helical region rather than the exact side chain chemistry.

The peptoid-based analogues also have the added advantages that they are less prone to aggregation in solution, protease degradation, and structural transformations than natural or synthetic SP-C analogues. The added stability is likely to be an advantage in a biomimetic SRT as it would ease the synthesis and purification as well as increase the shelf life and bioavailability after administration of the SRT. While it has been shown that excessive accumulation of misfolded SP-C in the airspaces is associated with pulmonary alveolar proteinosis, specific protease degradation sites can be engineered in the analogues, aiding their clearance from the airways should it be determined that these analogues are not biocompatible (*29*).

Taken together, this study has shown that peptoid-based mimics of SP-C are able to exhibit biophysical activities highly similar to that of the SP-C peptide when combined with a biomimetic phospholipid formulation. It was also found that the same design considerations occurring in the peptide are also applicable in the development of peptoid-based mimics of SP-C. Specifically, the surface activity of the peptoid-based compounds was found to be dependent upon the conservation of the basic amphipathic sequence patterning and the maintenance of a hydrophobic helical region of approximately 14 *N*spe residues in length and that the critical feature of the carboxy-terminal region of SP-C is its rigid helical structure and overall hydrophobic content, enabling the molecule to be anchored in the lipid film. Therefore, the results observed are promising for the development of a synthetic biomimetic peptoid-based lung surfactant formulation for the treatment of RDS or other medical applications.

ACKNOWLEDGMENT

We thank Mark Johnson and Ronald Zuckermann for their assistance. N.J.B. acknowledges support from the NIH Biotechnology Training Program. We also acknowledge use of the Keck Biophysics facility at Northwestern University for CD measurements.

REFERENCES

1. Notter, R. H. (2000) *Lung Surfactants: Basic Science and Clinical Applications*, Marcel Dekker, New York.
2. Veldhuizen, R., Nag, K., Orgeig, S., and Possmayer, F. (1998) *Biochim. Biophys. Acta 1408*, 90−108.
3. Hall, S. B., Venkitaraman, A. R., Whitsett, J. A., Holm, B. A., and Notter, R. H. (1992) *Am. Rev. Respir. Dis. 145*, 24−30.
4. Wang, Z. D., Hall, S. B., and Notter, R. H. (1996) *J. Lipid Res. 37*, 790−798.
5. Halliday, H. L. (1996) *J. Perinat. Med. 24*, 417−26.
6. Wu, C. W., and Barron, A. E. (2002) in *Biomimetic Materials and Design: Interactive Biointerfacial Strategies, Tissue Engineering, and Drug Delivery* (Dillow, A. K., and Lowman, A. M., Eds.) pp 565−633, Marcel Dekker, New York.
7. Robertson, B., Johansson, J., and Curstedt, T. (2000) *Mol. Med. Today 6*, 119−124.
8. Whitelaw, A. (1996) *J. Perinat. Med. 24*, 427−435.
9. Moya, F. R., Hoffman, D. R., Zhao, B., and Johnston, J. M. (1993) *Lancet 341*, 858−860.
10. Long, W. (1993) *Semin. Perinatol. 17*, 275−284.
11. Davis, A. J., Jobe, A. H., Hafner, D., and Ikegami, M. (1998) *Am. J. Respir. Crit. Care Med. 157*, 553−559.
12. Johansson, J., Some, M., Linderholm, B. M., Almlen, A., Curstedt, T., and Robertson, B. (2003) *J. Appl. Physiol. 95*, 2055−2063.
13. Sinha, S. K., Lacaze-Masmonteil, T., Soler, A. V. I., Wiswell, T. E., Gadzinowski, J., Hajdu, J., Bernstein, G., and d'Agostino, R. (2005) *Pediatrics 115*, 1030−1038.
14. Weaver, T. E. (1998) *Biochim. Biophys. Acta 1408*, 173−179.
15. Curstedt, T., Johansson, J., Persson, P., Eklund, A., Robertson, B., Lowenadler, B., and Jornvall, H. (1990) *Proc. Natl. Acad. Sci. U.S.A. 87*, 2985−2989.
16. Johansson, J., Szyperski, T., Curstedt, T., and Wuthrich, K. (1994) *Biochemistry 33*, 6015−6023.
17. Vandenbussche, G., Clercx, A., Curstedt, T., Johansson, J., Jornvall, H., and Ruysschaert, J. M. (1992) *Eur. J. Biochem. 203*, 201−209.
18. Creuwels, L., Boer, E. H., Demel, R. A., Vangolde, L. M. G., and Haagsman, H. P. (1995) *J. Biol. Chem. 270*, 16225−16229.
19. Bi, X. H., Flach, C. R., Perez-Gil, J., Plasencia, I., Andreu, D., Oliveira, E., and Mendelsohn, R. (2002) *Biochemistry 41*, 8385−8395.
20. Flach, C. R., Gericke, A., Keough, K. M. W., and Mendelsohn, R. (1999) *Biochim. Biophys. Acta 1416*, 11−20.
21. Qanbar, R., Cheng, S., Possmayer, F., and Schurch, S. (1996) *Am. J. Physiol. 15*, 572−580.
22. Wang, Z. D., Gurel, O., Baatz, J. E., and Notter, R. H. (1996) *J. Biol. Chem. 271*, 19104−19109.
23. Gustafsson, M., Palmblad, M., Curstedt, T., Johansson, J., and Schurch, S. (2000) *Biochim. Biophys. Acta 1466*, 169−178.
24. Oosterlakendijksterhuis, M. A., Haagsman, H. P., Vangolde, L. M. G., and Demel, R. A. (1991) *Biochemistry 30*, 10965−10971.
25. Taneva, S. G., and Keough, K. M. W. (1994) *Biochemistry 33*, 14660−14670.

26. Alonso, C., Waring, A., and Zasadzinski, J. A. (2005) *Biophys. J. 89*, 266−273.
27. Szyperski, T., Vandenbussche, G., Curstedt, T., Ruysschaert, J. M., Wuthrich, K., and Johansson, J. (1998) *Protein Sci. 7*, 2533−2540.
28. Johansson, J., Gustafsson, M., Palmblad, M., Zaltash, S., Robertson, B., and Curstedt, T. (1998) *Biol. Neonate 74*, 9−14.
29. Gustafsson, M., Thyberg, J., Naslund, J., Eliasson, E., and Johansson, J. (1999) *FEBS Lett. 464*, 138−142.
30. Takei, T., Hashimoto, Y., Aiba, T., Sakai, K., and Fujiwara, T. (1996) *Biol. Pharm. Bull. 19*, 1247−1253.
31. Nilsson, G., Gustafsson, M., Vandenbussche, G., Veldhuizen, E., Griffiths, W. J., Sjovall, J., Haagsman, H. P., Ruysschaert, J. M., Robertson, B., Curstedt, T., and Johansson, J. (1998) *Eur. J. Biochem. 255*, 116−124.
32. Ikegami, M., and Jobe, A. H. (1998) *Pediatr. Res. 44*, 860−864.
33. Johansson, J., Curstedt, T., and Robertson, B. (2001) *Pediatr. Pathol. Mol. Med. 20*, 501−518.
34. Wu, C. W., Seurynck, S. L., Lee, K. Y., and Barron, A. E. (2003) *Chem. Biol. 10*, 1057−1063.
35. Seurynck, S. L., Patch, J. A., and Barron, A. E. (2005) *Chem. Biol. 12*, 77−88.
36. Miller, S. M., Simon, R. J., Ng, S., Zuckermann, R. N., Kerr, J. M., and Moos, W. H. (1995) *Drug Dev. Res. 35*, 20−32.
37. Kirshenbaum, K., Barron, A. E., Goldsmith, R. A., Armand, P., Bradley, E. K., Truong, K. T. V., Dill, K. A., Cohen, F. E., and Zuckermann, R. N. (1998) *Proc. Natl. Acad. Sci. U.S.A. 95*, 4303−4308.
38. Wu, C. W., Sanborn, T. J., Huang, K., Zuckermann, R. N., and Barron, A. E. (2001) *J. Am. Chem. Soc. 123*, 6778−6784.
39. Sanborn, T. J., Wu, C. W., Zuckerman, R. N., and Barron, A. E. (2002) *Biopolymers 63*, 12−20.
40. Clercx, A., Vandenbussche, G., Curstedt, T., Johansson, J., Jornvall, H., and Ruysschaert, J. F. (1995) *Eur. J. Biochem. 229*, 465−472.
41. Hosia, W., Johansson, J., and Griffiths, W. J. (2002) *Mol. Cell. Proteomics 1*, 592−597.
42. Zuckermann, R. N., Kerr, J. M., Kent, S. B. H., and Moos, W. H. (1992) *J. Am. Chem. Soc. 114*, 10646−10647.
43. Whitmore, L., and Wallace, B. A. (2004) *Nucleic Acids Res. 32*, 668−673.
44. Lobley, A., Whitmore, L., and Wallace, B. A. (2002) *Bioinformatics 18*, 211−212.
45. Sreerama, N., Venyaminov, S. Y., and Woody, R. W. (1999) *Protein Sci. 8*, 370−380.
46. Alig, T. F., Warriner, H. E., Lee, L., and Zasadzinski, J. A. (2004) *Biophys. J. 86*, 897−904.
47. Bringezu, F., Ding, J. Q., Brezesinski, G., and Zasadzinski, J. A. (2001) *Langmuir 17*, 4641−4648.
48. Gopal, A., and Lee, K. Y. C. (2001) *J. Phys. Chem. B 105*, 10348−10354.
49. Seurynck, S. L., Brown, N. J., Wu, C. W., Germino, K. W., Kohlmeir, E. K., Ingenito, E. P., Glucksberg, M. R., Barron, A. E., and Johnson, M. (2005) *J. Appl. Physiol. 99*, 624−633.
50. Tanaka, Y., Takei, T., Aiba, T., Masuda, K., Kiuchi, A., and Fujiwara, T. (1986) *J. Lipid Res. 27*, 475−485.
51. Putz, G., Goerke, J., Taeusch, H. W., and Clements, J. A. (1994) *J. Appl. Physiol. 76*, 1425−1431.
52. Wu, C. W., Kirshenbaum, K., Sanborn, T. J., Patch, J. A., Huang, K., Dill, K. A., Zuckermann, R. N., and Barron, A. E. (2003) *J. Am. Chem. Soc. 125*, 13525−13530.
53. Johansson, J., Curstedt, T., and Robertson, B. (1996) *Acta Paediatr. 85*, 642−646.
54. Mayer-Fligge, P., Volz, J., Kruger, U., Sturm, E., Gernandt, W., Schafer, K. P., and Przybylski, M. (1998) *J. Pept. Sci. 4*, 355−363.
55. Yousefi-Salakdeh, E., Johansson, J., and Stromberg, R. (1999) *Biochem. J. 343*, 557−562.
56. Wu, C. W., Sanborn, T. J., Zuckermann, R. N., and Barron, A. E. (2001) *J. Am. Chem. Soc. 123*, 2958−2963.
57. Rabanal, F., Ludevid, M. D., Pons, M., and Giralt, E. (1993) *Biopolymers 33*, 1019−1028.
58. Seurynck-Servoss, S. L., Brown, N. J., Dohm, M. T., Wu, C. W., and Barron, A. E. (2007) *Colloids Surf., B 57*, 37−55.
59. Lee, K. Y. C., Gopal, A., von Nahmen, A., Zasadzinski, J. A., Majewski, J., Smith, G. S., Howes, P. B., and Kjaer, K. (2002) *J. Chem. Phys. 116*, 774−783.
60. Ding, J. Q., Warriner, H. E., and Zasadzinski, J. A. (2002) *Phys. Rev. Lett. 88*, 168102.
61. Takamoto, D. Y., Lipp, M. M., von Nahmen, A., Lee, K. Y. C., Waring, A. J., and Zasadzinski, J. A. (2001) *Biophys. J. 81*, 153−169.
62. vonNahmen, A., Schenk, M., Sieber, M., and Amrein, M. (1997) *Biophys. J. 72*, 463−469.
63. Nakorn, P. N., Meyer, M. C., Flach, C. R., Mendelsohn, R., and Galla, H. J. (2007) *Eur. Biophys. J., Biophys. Lett. 36*, 477−489.
64. Kruger, P., Baatz, J. E., Dluhy, R. A., and Losche, M. (2002) *Biophys. Chem. 99*, 209−228.
65. Otis, D. R., Ingenito, E. P., Kamm, R. D., and Johnson, M. (1994) *J. Appl. Physiol. 77*, 2681−2688.

BI7021975